Observational constraints on the chemistry of isoprene nitrates over the eastern United States

Larry W. Horowitz, Arlene M. Fiore, and George P. Milly

NOAA Geophysical Fluid Dynamics Laboratory, Princeton, NJ

Ronald C. Cohen, Anne Perring, and Paul J. Wooldridge

Department of Chemistry, UC Berkeley, Berkeley , CA

Peter G. Hess, Louisa K. Emmons, Jean-François Lamarque

Atmospheric Chemistry Division, National Center for Atmospheric Research, Boulder, CO

Submitted to *Journal of Geophysical Research*

July 3, 2006

Abstract

We constrain uncertainties in the chemistry of isoprene nitrates using chemical transport model simulations in conjunction with observations over the eastern United States from the International Consortium for Atmospheric Research on Transport and Transformation (ICARTT) field campaign during summer 2004. In the model, the combination of a 4% yield of isoprene nitrate production from the reaction of isoprene hydroxyperoxy radicals with NO, a recycling of 40% NO_x when isoprene nitrates react with OH, and a fast dry deposition rate of isoprene nitrates best reproduces observed boundary layer concentrations of organic nitrates and their correlation with ozone. We also identify a set of plausible values for these parameters, based on additional simulations showing reasonable agreement with the boundary layer observations. We find that ~50% of the isoprene nitrate production in the model occurs via reactions of isoprene (or its oxidation products) with the NO_3 radical, but note that the isoprene nitrate yield from this pathway is highly uncertain. Isoprene nitrates are shown to have a major impact on the nitrogen oxide (NO_x = NO + NO_2) budget in the U.S. continental boundary layer, consuming 15-19% of the emitted NO_x, of which 3-5% is recycled back to NO_x and the remainder is exported as isoprene nitrates (3-4%) or deposited (8-11%). The underestimate of free tropospheric concentrations of organic nitrates in all simulations requires future investigation.

1. Introduction

Photochemical oxidation of volatile organic compounds (VOCs) in the presence of nitrogen oxides (NO_x = NO + NO_2) contributes to the production of ozone. Over the eastern United States during summer, chemical reactivity and subsequent ozone production are dominated by isoprene (2-methyl-1,3-butadiene), a biogenic VOC with large emissions that reacts rapidly with OH [e.g., *Trainer et al.,* 1987]. Isoprene oxidation also modulates the partitioning and fate of reactive nitrogen within the continental boundary layer [e.g., *Horowitz et al.*, 1998; *Houweling et al.*, 1998].

Recent modeling studies have demonstrated that ozone concentrations and reactive nitrogen partitioning are sensitive to uncertainties in the isoprene chemical oxidation pathways [*Horowitz et al.*, 1998; *von Kuhlmann* et al., 2004; *Fiore* et al., 2005; *Wu et al.*, 2006]. Specific uncertainties include the magnitude and spatial distribution of isoprene emissions, the yield and fate of isoprene nitrates, and the fate of organic hydroperoxides. Previous studies suggest that surface ozone is only weakly sensitive to the uncertainties in organic hydroperoxides (up to 2-3 ppbv), while the choice of isoprene emissions inventory can have large local or regional effects (up to 15 ppbv ozone locally) [*von Kuhlmann et al.*, 2004; *Fiore et al.*, 2005]. We focus in this paper on the uncertainties in isoprene nitrate chemistry, which have been shown to affect surface ozone (by up to 10 ppbv) and NO_x (by up to 10%) [*Horowitz et al.*, 1998; *von Kuhlmann et al.*, 2004; *Fiore et al.*, 2005]. We analyze chemical transport model simulations in conjunction with observations from the International Consortium for Atmospheric Research on Transport and Transformation (ICARTT) field campaign [*Fehsenfeld et al.*, 2006; *Singh et al.,* 2006] conducted

in summer 2004 to constrain the uncertainties in isoprene nitrate chemistry and examine the implications of these constraints for the NO_x budget and ozone concentrations over the eastern United States.

When isoprene is oxidized by OH, six different isomeric hydroxyperoxy (RO_2) radicals are formed (after the addition of O_2). Under high-NO_x conditions these radicals typically react with NO, forming primarily hydroxalkoxy (RO) radicals with a minor channel leading to the production of organic hydroxynitrates ($RONO_2$, "isoprene nitrates") [e.g., *Chen et al.*, 1998]. Laboratory studies have estimated the yield of isoprene nitrates from the RO_2+NO reaction to range from 4.4% to 15% [*Chen et al.*, 1998; *Tuazon and Atkinson*, 1990 (corrected as discussed by *Paulson et al.*, 1992); *Chuong and Stevens*, 2002; *Sprengnether et al.*, 2002]. Model studies have shown that tropospheric ozone production and surface concentrations are sensitive to the isoprene nitrate yield [*von Kuhlmann et al.*, 2004; *Wu et al.*, 2006].

The oxidation of isoprene by NO_3, which occurs primarily at night, leads to the production of another set of isoprene nitrates. This pathway proceeds by addition of NO_3 to one of the double bonds in isoprene followed by addition of O_2 to form nitrooxyalkyl peroxy radicals. These radicals can then either undergo subsequent reactions to form stable organic nitrates or decompose to release NO_x; the relative amounts of organic nitrates versus released NO_x are poorly known [e.g., *Paulson and Seinfeld*, 1992; *Fan and Zhang*, 2004]. The isoprene nitrates formed by the isoprene-NO_3 channel are expected to be aldehydic [*Paulson and Seinfeld*, 1992] or ketonic nitrates [*Fan and Zhang*, 2004], as opposed to the hydroxynitrates formed from the isoprene-OH channel. The importance of the NO_3 versus OH pathways for isoprene nitrate

production is also uncertain, but a modeling study suggests that > 60% of isoprene nitrates may be produced through the isoprene-NO_3 channel [*von Kuhlmann et al.*, 2004].

Isoprene nitrates contain a double bond, so they are highly reactive towards OH, ozone, and NO_3. Reaction with OH is expected to be the major chemical loss. Estimates of the reaction rate constant for isoprene nitrates + OH range from (1.3-9)x10^{-11} molec^{-1} cm^3 s^{-1} [*Paulson and Seinfeld*, 1992; *Shepson et al.*, 1996, *Chen et al.*, 1998; *Giacopelli et al.*, 2005], although some model studies have assumed rate constants as low as 6.8x10^{-13} [*Brasseur et al.*, 1998].

The products of the isoprene nitrate + OH reaction have not been directly measured. *Paulson and Seinfeld* [1992] suggested that this reaction should release NO_x, while other studies conclude that the reaction of some isomers will lead to the production of secondary multifunctional organic nitrates [*Grossenbacher et al.*, 2001; *Giacopelli et al.*, 2005]. The release of NO_x by this reaction or its continued sequestration in organic nitrates can significantly alter the extent to which isoprene chemistry acts as a sink for NO_x [e.g., *Chen et al.*, 1998; *Horowitz et al.*, 1998], with up to ~10% effects on surface ozone concentrations [*von Kuhlmann et al.*, 2004; *Fiore et al.*, 2005].

Removal of isoprene nitrates by wet and dry deposition provides a permanent sink for atmospheric NO_x. The rate of wet deposition depends on the Henry's law constant, which has been estimated by analogy with comparable species to range from H(298K) = 6.0x10^3 M atm^{-1} [*Shepson et al.*, 1996] to 1.7x10^4 [*von Kuhlmann et al.*, 2004]. Estimates of the dry deposition velocity of isoprene nitrates range from that of PAN (0.4-0.65 cm s^{-1}) [*Shepson et al.*, 1996;

Giacopelli et al., 2005] to that of HNO_3 (4-5 cm s^{-1}) [*Rosen et al.*, 2004]. Using the slower deposition estimates and an OH rate constant of $1.3x10^{-11}$ $molec^{-1}$ cm^3 s^{-1}, *Shepson et al.* [1996] predicted that reaction with OH should dominate isoprene nitrate loss, with an overall atmospheric lifetime of ~18h.

The ICARTT multi-agency international field campaign conducted during summer 2004 included measurements of isoprene, its oxidation products, reactive nitrogen compounds, and ozone over the eastern United States. Since chemistry in this region and season is strongly influenced by emissions of both biogenic isoprene and anthropogenic NO_x, the ICARTT campaign presents an opportunity to study the effect of isoprene on reactive nitrogen partitioning and ozone production. We analyze the ICARTT observations in conjunction with a 3-dimensional chemical transport model to identify new constraints on the chemistry of isoprene nitrates. The model is described in Section 2, and evaluated with observations in Section 3. In Section 4, we examine the sensitivity of our results to uncertainties in isoprene nitrate chemistry, derive observational constraints on this chemistry, and discuss the implications for the NO_x budget over the eastern United States. Conclusions are presented in Section 5.

2. Model description

We simulate the chemistry during the ICARTT period (July-August 2004) using the Model of Ozone and Related Chemical Tracers, version 4 (MOZART-4) chemical transport model [*Emmons et al.*, 2006, manuscript in preparation]. This model is an updated version of the MOZART-2 model [*Horowitz et al.*, 2003] with aerosol chemistry based on that of *Tie et al.*

[2005]. In MOZART-4, photolysis rates are calculated interactively to account for absorption and scattering by aerosols and clouds with Fast-TUV [*Madronich and Flocke*, 1998; *Tie et al.*, 2005]. The influx of O_3 from the stratosphere is prescribed using the SYNOZ technique (500 Tg yr^{-1}) [*McLinden et al.*, 2000]. The prescribed monthly mean deposition velocities for O_3 and PAN have been increased based on those used by *Bey et al.* [2001]. The mechanism now represents the chemistry of higher alkanes with the "bigalk" (C_5H_{12}) tracer, a lumped species representing the butanes, pentanes, and hexanes. Higher alkenes are included as "bigene" (C_4H_8), a lumped species representing mostly 2-methylpropene and 2-butene. An additional new species, "toluene" (C_7H_8), is a lumped aromatic compound representing mostly benzene, toluene, and the xylenes. Additional oxidation products of the above species have also been added. Updates to the chemistry in MOZART-4 are more fully described by *Emmons et al.* [2006].

The isoprene oxidation mechanism in our BASE simulation is shown in Table 1. In Section 4, we evaluate the sensitivity of our results to the assumptions in our BASE isoprene mechanism described here, using the additional model simulations described in Table 2. The treatment of isoprene nitrates has been modified from that in MOZART-2 [*Horowitz et al.*, 2003]. The yield of ONITR from the addition branch of the ISOPO2 + NO reaction has been decreased from 8% in MOZART-2 to 4% [e.g., *Chen et al.*, 1998] in the BASE simulation. A new species (XNITR in Table 1) represents secondary multifunctional organic nitrates. The reaction of primary isoprene nitrates (ONITR) with OH recycles 40% of NO_x, rather than 100% as in MOZART-2, with the balance forming XNITR based on recent studies suggesting that this reaction produces some secondary nitrates [e.g., *Grossenbacher et al.*, 2001; *Giacopelli et al.*, 2005]. XNITR has no chemical losses in our mechanism, as its further reactions are assumed to

convert it to more highly substituted organic nitrates. The reaction ONITR + NO_3 is also assumed to produce XNITR. Note that the carbonyl nitrates produced from the isoprene-NO_3 channel (via ISOPNO3) are represented in our mechanism by the same ONITR species as the hydroxynitrates from the isoprene-OH channel. This simplifying assumption neglects any differences in reactivity or deposition between these two different classes of isoprene nitrates.

The oxidation scheme for monoterpenes, represented by α-pinene, has been updated to reflect recent laboratory data (see Table 1 and *Emmons et al.* [2006]). We assume that terpene oxidation produces organic nitrates with an 18% yield from the reaction of terpene peroxy radicals (TERPO2) with NO, based on estimates by *Nozière et al.* [1999]. We note that this yield is considerably higher than the ~1% yield estimated by *Aschmann et al.* [2002], although *Aschmann et al.* acknowledged the possibility that their results were biased low by aerosol formation or loss to the chamber wall.

Global emissions were specified as by *Horowitz et al.* [2003], with anthropogenic emissions based on EDGAR v2.0 [*Olivier et al.,* 1996] and biomass burning from *Müller* [1992] and *Hao and Liu* [1994] with emission ratios from *Andreae and Merlet* [2001]. Isoprene and monoterpene emissions are calculated interactively based on temperature, sunlight, and vegetation type using algorithms from the Model of Emissions of Gases and Aerosols from Nature (MEGAN v.0) [*Guenther et al.,* 2006]. Over North America during summer, we use updated anthropogenic surface emissions based on the EPA National Emissions Inventory (NEI99, version 3, http://www.epa.gov/ttn/chief/net/1999inventory.html) [S. McKeen, personal communication, 2004], and the daily biomass burning emission inventory developed by *Turquety*

et al. [2006]. Biomass burning emissions are distributed vertically up to 4 km altitude, with 70% of the emissions occurring below 2 km. Surface emissions over the eastern United States (24-52°N, 62.5-97.5°W) in July 2004 total 0.52 TgN NO_x, 7.8 Tg CO, 3.7 TgC isoprene, and 0.91 TgC terpenes.

Meteorological fields are provided by the NCEP Global Forecast System (GFS) every three hours. The model resolution is 1.9° latitude x 1.9° longitude, with 64 vertical levels, and a dynamical and chemical timestep of 15 minutes. The BASE model simulation was conducted from December 2003 through the ICARTT period (July-August 2004). Sensitivity simulations (Section 4.1) begin in May 2004, allowing for a two-month spinup period sufficient to capture changes in summertime continental boundary layer chemistry.

3. Results from base simulation

3.1 Evaluation with ICARTT observations

We evaluate the results of the MOZART-4 BASE simulation with observations made on board the NASA DC-8 [*Singh et al.*, 2006a] and NOAA WP-3D [*Fehsenfeld et al.*, 2006] aircraft during ICARTT. Simulated concentrations are sampled every minute along the flight tracks of the two aircraft and then averaged onto the model grid for each flight. The two aircraft pursued different sampling strategies: the DC-8 typically aimed to sample regionally representative air masses, while the WP-3D often sampled local plumes from urban outflow or power plants. Thus,

we expect our model to simulate better the tracer concentrations measured by the DC-8, whereas the local plumes sampled by the WP-3D are likely to be poorly represented due to their fine spatial scale relative to the model resolution.

Comparisons of selected species, including isoprene, isoprene oxidation products, ozone, and ozone precursors, below 2km in the eastern United States are presented in Figure 1. Isoprene concentrations show little bias, but are poorly correlated with observations (r^2 = 0.09 and mean bias = +15% for NASA, r^2 = 0.32 and bias = -16% for NOAA), most likely due to the short lifetime of isoprene and the high spatial variability of its emissions. The first generation isoprene oxidation products methylvinyl ketone and methacrolein, which have longer atmospheric lifetimes, are better simulated by the model (r^2 = 0.50, bias = -10%). Monoterpene concentrations are underestimated by almost a factor of 2, but correlate reasonably well with observations (r^2 = 0.33). Overall, we conclude that MEGAN captures the magnitude and large-scale spatial pattern of isoprene emissions, but may underestimate terpene emissions.

Boundary-layer concentrations of ozone are slightly overestimated (mean bias = +7.1% for NASA, +3.0% for NOAA) and moderately correlated with observations (r^2 = 0.31 for NASA, 0.17 for NOAA). CO and NO_x are moderately well correlated with observations (r^2 = 0.43 and 0.12 for CO from NASA and NOAA, respectively, r^2 = 0.36 for NO_x from NASA), with an average model overestimate of ~15% for CO and ~30% for NO_x. Secondary oxidation products PAN and formaldehyde (CH_2O) are well correlated with the observations, but PAN tends to be overestimated in the boundary layer. PAN concentrations in the free troposphere have little mean bias (not shown). Simulated organic nitrates (ONITR + XNITR + ISOPNO3 + other organic

nitrates) are slightly overestimated versus the observed total alkyl- and hydroxyalkyl-nitrates (ΣANs) which were measured by thermal-dissociation laser-induced fluorescence (TD-LIF) [*Day et al.*, 2002] (bias = +20%, r^2=0.20). Concentrations of HNO_3 and H_2O_2 are poorly correlated with observations, suggesting possible model errors in wet deposition.

With the exception of organic nitrates, the agreement between simulated and observed concentrations for the species evaluated in Figure 1 is relatively insensitive to assumptions about isoprene nitrate chemistry (at least to within model biases), as represented by the sensitivity simulations in Section 4.1. We thus use only the observed ΣAN concentrations to provide constraints on the chemistry of isoprene nitrates (Section 4.2). We begin by examining the budget of isoprene nitrates in Section 3.2.

3.2 Isoprene nitrate budget

Budgets for isoprene nitrate (ONITR+XNITR) production and loss in the eastern United States boundary layer during July 2004 are presented in Figure 2. In the BASE simulation, half of the isoprene nitrate production occurs through the NO_3 pathway, in which isoprene reacts with NO_3 to form ISOPNO3, which can then react with NO, NO_3, or HO_2 to form carbonyl nitrates. These carbonyl nitrates, represented in our mechanism by the same ONITR species as the hydroxynitrates formed from the isoprene-OH pathway, are assumed to form with a yield of 79.4% from all ISOPNO3 reaction pathways (see Table 1) [*Horowitz et al.*, 2003]. The large contribution of this pathway to isoprene nitrate production, despite the small fraction of isoprene oxidized via this pathway (~6%), agrees well with the findings of *von Kuhlmann et al.* [2004].

About 25% of the isoprene nitrate production occurs via the reaction ISOPO2 + NO, which produces ONITR with a 4% yield in this simulation. Each of the reactions MACRO2+NO and TERPO2+NO (TERPO2 is formed by terpenes+OH or terpenes+NO_3) yields another 12-14%. This partitioning of organic nitrate sources is similar to that calculated by *Cleary et al.* [2005] for the suburbs of Sacramento, CA. Note that we assume the same ONITR yield from terpenes+OH and terpenes+NO_3 (18%), while in the case of isoprene we include a much higher yield from isoprene+NO_3 (79.4%) than for isoprene+OH (4% in the BASE case). The loss of isoprene nitrates in the BASE simulation occurs largely by dry deposition (50%) and reaction with OH (26%), with minor loss by transport (19%) and wet deposition (5%).

4. Isoprene nitrate sensitivity analysis

In this section, we examine the sensitivity of our model results to assumptions concerning the production and loss of isoprene nitrates, using the additional simulations in Table 2. In particular, we examine the sensitivity of isoprene nitrates to the assumed yield, OH reaction rate, recycling of NO_x, and deposition rate. We place constraints on the isoprene nitrate chemistry based on boundary layer observations of ΣAN, and describe the effects of isoprene nitrates on the NO_x budget over the eastern United States.

4.1 Sensitivity simulations

The production of isoprene nitrates following the oxidation of isoprene by OH depends on the yield of these nitrates from the reaction of the isoprene peroxy radicals (ISOPO2 in Table 1) with NO. We conduct sensitivity simulations in which the yield is increased from the BASE case value of 4% [*Chen et al.*, 1998] to 8%, as assumed by *Fan and Zhang* [2004]. In the simulations with an 8% yield (8% and 8%_slowOH in Table 2), the production of isoprene nitrates via the ISOPO2+NO pathway doubles compared to the runs with a 4% yield (BASE and 4%_slowOH), but production via other pathways is relatively unchanged (Figure 2). Thus, the total production of isoprene nitrates increases by ~22% in these simulations.

The chemical loss of isoprene nitrates (ONITR) is primarily through reaction with OH. Our BASE simulation assumes a rate constant of $k = 4.5 \times 10^{-11}$ molec^{-1} cm^3 s^{-1} for isoprene nitrates + OH [*Emmons et al.*, 2006], within the range of $(3\text{-}9) \times 10^{-11}$ molec^{-1} cm^3 s^{-1} estimated by *Giacopelli et al.* [2005] using the method of *Kwok and Atkinson* [1995]. There is evidence that the *Kwok and Atkinson* [1995] method may overestimate the rate constant for OH reaction with hydroxyalkyl nitrates by a factor of 2-21 [*Neeb*, 2000; *Treves and Rudich*, 2003], so we also consider a lower rate constant of $k = 1.3 \times 10^{-11}$ molec^{-1} cm^3 s^{-1} (simulations 4%_slowOH, 8%_slowOH), similar to that used in several other studies [*Shepson et al.*, 1996; *Chen et al.*, 1998; *Pöschl et al.*, 2000; *Horowitz et al.*, 2003]. In these simulations, the photolysis rate for ONITR, J(ONITR), is also decreased from its BASE case value of J(CH_3CHO) to J(HNO_3). The ONITR+OH reaction accounts for ~26% of the isoprene nitrate loss when a fast reaction rate is assumed (BASE and 8%), but only 21% when a slower rate is used (4%_slowOH and

8%_slowOH in Figure 2). Photolysis of ONITR is a minor loss in all simulations, accounting for ~2% of the isoprene nitrate loss in the BASE and 8% simulations and only ~1% in 4%_slowOH and 4%_slowOH. The overall lifetime of isoprene nitrates (ONITR+XNITR+ISOPNO3) increases by only 8-9% in the simulations with slower ONITR loss (Table 2).

When isoprene nitrates (ONITR) react with OH, the reactive nitrogen can be recycled to NO_x or retained as XNITR. In the BASE case, we assume a NO_x recycling efficiency of 40%. Since this recycling efficiency is uncertain [*Paulson and Seinfeld,* 1992; *Chen et al.*, 1998; *Grossenbacher et al.*, 2001, *Giacopelli et al.,* 2005], we include three sensitivity simulations in which the recycling is varied from extreme values of 0% (4%_0%NOx in Table 2) to 100% (4%_100%NOx and 8%_slowOH_100%NOx). When the recycling is completely turned off, the ONITR+OH reaction ceases to be a sink for isoprene nitrates and instead produces 100% XNITR. As a result, the burden of isoprene nitrates increases by 44% (Table 2) and losses via dry and wet deposition increase by ~30% and ~50%, respectively (Figure 2). When the recycling is increased from 40% to 100%, the loss of isoprene nitrates from ONITR+OH increases proportionally by a factor of 2.5 to account for 51-64% of the total loss, causing the isoprene nitrate burden and lifetime to decrease by more than a factor of 2.

The final sensitivity we examine is the rate at which isoprene nitrates (ONITR and XNITR) are lost by deposition. In the BASE simulation, we assume that isoprene nitrates deposit rapidly, with a dry deposition velocity equal to that of HNO_3 and a wet deposition rate (Henry's Law constant of $H_{298} = 7.51 \times 10^3$ M atm^{-1}) similar to that assumed by *Shepson et al.* [1996]. Since dry deposition dominates over wet deposition as a loss pathway from the boundary layer

(see Section 3.2 and Figure 2), we examine the sensitivity of our results to the removal rate by decreasing the dry deposition velocity of isoprene nitrates by a factor of ~20 to that of PAN (simulations 4%_slowDD, 8%_slowDD) [*Shepson et al.*, 1996; *Giacopelli et al.*, 2005]. In these simulations with slow dry deposition, the isoprene nitrate burden and lifetime increase by a factor of 2 (Table 2) and loss via export and the ONITR+OH reaction increase in importance, accounting for up to 46% and 34% of the total loss, respectively (Figure 2).

4.2 Constraints from observations

The sensitivity simulations described above (Section 4.1 and Table 2) most dramatically affect the concentrations of isoprene nitrates, with only small impacts on the other species evaluated in Section 3.1. Previous calculations have shown that biogenically derived nitrates are the primary source of ΣANs in Sacramento [*Cleary et al.*, 2005], in eastern Pennsylvania [*Trainer et al.*, 1991], and rural Michigan and Alabama [*Sillman and Samson*, 1995], but not in Houston, Texas [*Rosen et al.*, 2004] The speciated (non-isoprene) alkyl nitrates measured from whole-air samples during ICARTT (by D. Blake) typically account for an average of only ~10% of the observed ΣANs, indicating that the ΣANs are primarily composed of larger compounds or multi-functional compounds such as the isoprene and terpene nitrates, consistent with the model results. A more detailed discussion of the comparison of individually measured nitrates to the observations of ΣANs will be presented in a forthcoming paper (A. Perring et al., manuscript in preparation). In this section, we utilize measurements of total alkyl- and hydroxyalkyl-nitrates (ΣANs) [*Day et al.*, 2002] during ICARTT to constrain the chemistry of isoprene nitrates.

Simulated organic nitrate concentrations (ONITR + XNITR + ISOPNO3 + other organic nitrates) are compared with observations of ΣANs in Figure 3. The mean organic nitrates simulated in the BASE case agree well with observed concentrations in the boundary layer, with a bias of +10-20%, whereas a small negative bias may have been expected based on the previously discussed underestimate of MVK+MACR (Figure 1). The model underestimates free tropospheric ΣAN by more than a factor of 2. The correlation of ozone with ΣANs provides an additional means of evaluating organic nitrate abundances because both organic nitrates and ozone are produced from the reactions of RO_2 radicals with NO, so the concentration ratio may normalize for any model errors in the absolute concentrations of RO_2 or in the rate of boundary layer ventilation. The BASE model reproduces the observed $\Delta O_3/\Delta\Sigma AN$ correlation slope (83.9 simulated, 81.7 observed), although the correlation is much stronger in the model (r=0.88 vs. 0.35 observed). This slope is similar to the relationship reported by *Day et al.* [2003] for a rural location in California and to those reported by *Rosen et al.* [2004] and *Cleary et al.* [2005] for urban areas in late afternoon. Based on the methodology of *Rosen et al.* [2004] and *Cleary et al.* [2005], a $\Delta O_3/\Delta\Sigma AN$ slope of 81.7 corresponds to an "effective ΣAN yield" of 2.4% from the complete mix of ozone-producing VOCs. An "effective ΣAN yield" of about a factor of two lower than the yield calculated from OH-initiated VOC chemistry in the daytime is similar to results reported by *Rosen et al.* [2004] and *Cleary et al.* [2005]. The 8% simulation overestimates ΣANs (+40% bias) and underestimates the $\Delta O_3/\Delta\Sigma AN$ slope (64.5).

The simulations with slower loss of ONITR via OH (4%_slowOH and 8%_slowOH) have 8-11% higher boundary layer concentrations (Figure 3) and burdens (Table 2) of ΣANs than the corresponding simulations with the faster ONITR+OH reaction rate, even though the

reaction rate constant was decreased by more than a factor of 3. This small response indicates that reaction with OH is a relatively small loss of isoprene nitrates compared with deposition, as demonstrated by the BASE isoprene nitrate budget in Section 3.2. The higher concentrations of ΣANs decrease the $\Delta O_3/\Delta\Sigma AN$ correlation slope, degrading agreement with observations.

When the reaction of ONITR+OH is allowed to recycle all of the NO_x (4%_100%NOx), boundary layer concentrations of ΣAN are underestimated by a factor of 4 or more. If we additionally assume an 8% yield of ONITR and the slow rate of ONITR+OH reaction, the ΣAN concentrations increase to 50-65% of observed values, but the $\Delta O_3/\Delta\Sigma AN$ correlation slope is still greatly overestimated (140.1). In both of the simulations with 100% recycling (4%_100%NOx, 8%_slowOH_100%_NOx), free tropospheric ΣAN concentrations are dramatically underestimated by a factor of 10 or more. On the other hand, if the ONITR+OH reaction is assumed to recycle no NO_x (4%_0%NOx), instead forming XNITR exclusively, ΣAN concentrations increase by 50% from the BASE case, leading to 70% overestimates of observed ΣAN and a large underestimate of $\Delta O_3/\Delta\Sigma AN$ (52.3).

In the final set of sensitivity simulation, the dry deposition velocity of isoprene nitrates is decreased from that of HNO_3 to that of PAN (simulations 4%_slowDD and 8%_slowDD). In these simulations, ΣAN concentrations increase by approximately a factor of 2, dramatically worsening agreement with observed ΣAN concentrations and $\Delta O_3/\Delta\Sigma AN$ correlation slopes in the boundary layer; simulated concentrations of ΣAN in the free troposphere approach observed values, but are still slightly underestimated. The discrepancy between simulated and observed ΣAN in the free troposphere is discussed further below.

Based on the comparisons with observed boundary-layer ΣANs and $\Delta O_3/\Delta\Sigma AN$, we find that the BASE simulation — with its 4% yield of isoprene nitrates from ISOPO2+NO, fast rate of isoprene nitrate-OH reaction, recycling of 40% NO_x, and fast loss by dry deposition — best matches observations of ΣAN concentrations and $\Delta O_3/\Delta\Sigma AN$ correlation slopes. The simulations with an 8% yield and/or slower reaction of ONITR+OH degrade agreement with observation somewhat. The simulations with slow dry deposition and those with either 0% or 100% NO_x recycling show the worst agreement with observations. Based on these results, we select the BASE case as the "best guess" set of model parameters, but also consider a range of uncertainty including the other simulations showing reasonable agreement with observations (4%_slowOH, 8%, 8%_slowOH).

Our best guess of a 4% yield of isoprene nitrates agrees well with the values measured by *Chen et al.* [1998], but is significantly lower than the values (up to 15%) from other studies [*Tuazon and Atkinson*, 1990; *Chuong and Stevens*, 2002; *Sprengnether et al.*, 2002]. The BASE case ONITR+OH rate constant of $k=4.5x10^{-11}$ $molec^{-1}$ cm^3 s^{-1} is within the range estimated by *Giacopelli et al.* [2005], but we find that the agreement with observations is only slightly degraded when the lower reaction rate of $k=1.3x10^{-11}$ is used (e.g., *Paulson and Seinfeld*, 1992; *Chen et al.*, 1998). We find that the assumption of 40% NO_x recycling from ONITR+OH gives the best agreement with observations, although a somewhat higher recycling rate could be supported, especially if the production yield of isoprene nitrates were higher. The degree of recycling has not been well constrained by previous studies, with *Paulson and Seinfeld* [1992] arguing that NO_x should be released from this reaction, but other studies suggesting the

formation of secondary multifunctional nitrates [*Grossenbacher et al.*, 2001; *Giacopelli et al.*, 2005]. Finally, our results suggest that isoprene nitrates are removed relatively quickly by dry deposition, as supported by observations from *Rosen et al.* [2004], but faster than suggested by [*Shepson et al.*, 1996; *Giacopelli et al.*, 2005].

Most of the analysis in this paper has focused on the chemistry of the continental boundary layer, where short-lived isoprene is abundant and isoprene nitrates are expected to dominate ΣAN. In the boundary layer, we find that the BASE simulation best reproduces the ICARTT observations of ΣAN concentrations and $\Delta O_3/\Delta\Sigma AN$ correlations. All of the simulations presented here, however, considerably underestimate ΣAN in the free troposphere. Those that most closely match the free tropospheric observations (4%_slowDD and 8%_slowDD; mean biases of -40% and -25%, respectively) overestimate ΣAN by factors of 2-3 (and underestimate the $\Delta O_3/\Delta\Sigma AN$ correlation slope by a factor of 2 or more) in the boundary layer. The simulations with 100% NO_x recycling (and no XNITR production) from ONITR+OH (4%_100%NOx and 8%_slowOH_100%NOx) underestimate free tropospheric concentrations by a factor of 10 or more, indicating that most of the organic nitrates in the model in the free troposphere are secondary multifunctional organic nitrates (XNITR).

The underestimate of ΣANs in all simulations could be due to other sources of organic nitrates in the free troposphere not represented in the model. The speciated alkyl nitrates measured during ICARTT, however, typically account for only ~10% of the observed ΣANs even in the free troposphere. Alternatively, the underestimate could be caused by insufficient vertical mixing out of the boundary layer in the model, which could also account for the model

overestimate of NO_x and CO in the boundary layer. Based on the correlation between isoprene nitrate export from the boundary layer (Figure 2) and free tropospheric ΣAN concentrations (Figure 3), we estimate that a monthly export flux of ~50-60 GgN could enable the model to reproduce observed free tropospheric ΣANs. High isoprene nitrate export only occurs in our simulations, however, when boundary layer ΣAN concentrations are strongly overestimated. Our model treats both aldehydic and hydroxy nitrates as a single species, whereas less efficient removal of the aldehydic nitrates by wet and dry deposition could increase export and improve the simulation of free tropospheric ΣANs. While increased boundary layer ventilation would decrease isoprene nitrate concentrations in the boundary layer, it would not be expected to alter the simulated ratio $\Delta O_3/\Delta\Sigma AN$ dramatically, suggesting that constraints derived above from boundary layer observations should be robust to a possible model bias in ventilation.

4.3 Implications for NO_x budget

We find that the formation of isoprene nitrates has a large effect on the NO_x budget in the summertime boundary layer. In the BASE simulation, which best agrees with the ΣAN and $\Delta O_3/\Delta\Sigma AN$ observations in the boundary layer (Figure 3), out of a total 519 GgN surface NO_x emissions from the eastern United States in July, 78 GgN (15% of emissions) cycles through isoprene nitrates. Once formed, 20 GgN (4% of emissions) is recycled from isoprene nitrates back to NO_x within the continental boundary layer, 43 GgN (8% of emissions) are removed permanently by dry and wet deposition, and 15 GgN (3% of emissions) are exported to the free troposphere as isoprene nitrates. For comparison, *Horowitz et al.* [1998] estimated that isoprene

nitrate net chemical production (production minus loss from recycling) accounted for 16% of NO_x emissions the eastern United States in summer, with deposition and export of isoprene nitrates equal to 14% and 1.5%, respectively. Because the model underestimates the ΣANs in the free troposphere, as discussed above in Section 4.2, it is possible that the export of ΣANs from the boundary layer is much larger than we calculate.

We estimate a range for the values above by considering those simulations that agree best with boundary layer observations of ΣANs and $\Delta O_3/\Delta\Sigma AN$ (Figure 3), excluding the simulations with slow dry deposition and with 0% and 100% NO_x recycling. We thus estimate an observationally constrained isoprene nitrate budget range of: production (78-96 GgN), recycling to NO_x (16-25 GgN), deposition (43-56 GgN), and export (15-19 GgN). Note that this constrained budget range is considerably narrower than the range that would be obtained if all sensitivity simulations were considered, especially for the loss terms. The full range of losses is: recycling to NO_x (0-51 GgN, 0-10% of NO_x emissions), deposition (16-56 GgN, 3-11%), and export (6-44 GgN, 1-8%). The full range of isoprene nitrate production (77-97 GgN, 15-19% of emissions) is similar to the constrained range above.

Isoprene nitrate chemistry affects ozone concentrations through its impact on the NO_x budget. Uncertainties in the isoprene nitrate chemistry can alter the mean ozone mixing ratios in the boundary layer by up to +2.9 ppbv (in simulation 4%_100NOx) and -1.9 ppbv (4%_0NOx) from their BASE case values (Figure 1), demonstrating that recycling of NO_x from isoprene nitrates can have almost a 5 ppbv impact on ozone. If we consider only the observationally

constrained simulations, the uncertainty range of mean ozone decreases to -1.8 to 0 ppbv from the BASE case.

5. Conclusions

We combine model simulations and observations from the ICARTT field campaign over the eastern United States during summer 2004 to constrain the chemistry of isoprene nitrates. Simulated concentrations of trace species generally match observations to within 30% in the U.S. boundary layer, except for NO_x (overestimated by ~30%) and PAN (overestimated by a factor of ~2); free tropospheric concentrations of these species do not show this overestimate. Additional simulations are conducted to examine the sensitivity of model results to assumptions about the following uncertain aspects of isoprene chemistry: isoprene nitrate production yield, chemical loss rate, NO_x recycling, and dry deposition. Observed concentrations of total hydroxyalkyl- and alkyl-nitrates (ΣANs) and the correlation of ozone with ΣANs are used to constrain the possible values of the above parameters. We find that our simulations with low deposition velocities for isoprene nitrates produce unacceptably high boundary layer concentrations of ΣANs. Extreme rates of NO_x recycling (0% or 100%) from the reaction of isoprene nitrates with OH lead to ΣAN concentrations that are strongly biased (high or low, respectively) compared with observations, but model results are relatively insensitive to the rate of this reaction. Finally, better agreement is obtained with a lower isoprene nitrate production yield of 4% than with a higher yield of 8%. The observations are best reproduced by the BASE simulation, which matches the mean observed ΣAN concentrations in the boundary layer within 10-20%, and the observed $\Delta O_3/\Delta\Sigma AN$ correlation slope (83.9 in the model, 81.7 in the observations).

Based on the evaluation of model results versus boundary layer observations, we find that the most likely values for the parameters considered are: an isoprene nitrate yield from ISOPO2+NO of 4%, recycling of about half of ONITR to NO_x in the reaction with OH, and fast removal of isoprene nitrates by dry deposition (at a rate similar to that of HNO_3). We also identify a range of plausible values for these parameters based on other simulations (4%_slowOH, 8%, 8%_slowOH). That is, an 8% yield of isoprene nitrates or a slower loss of isoprene nitrates by reaction with OH slightly degrades agreement with observations, but cannot be ruled out by this study. Of course, the set of sensitivity experiments conducted here are not exhaustive of all possible values and combinations of the parameters. For example, an 8% production yield of ONITR from ISOPO2+NO together with a somewhat higher rate of NO_x recycling from ONITR+OH, might match observational constraints as well as the BASE simulation.

We find that the NO_3 production pathway accounts for 50% of the total organic nitrate production in the BASE case (with a range of ~40-50% in the other observationally constrained simulations, depending on the production yield of ONITR from ISOPO2+NO). The loss of isoprene nitrates occurs primarily by dry deposition (50% in BASE, and up to 54% in simulations using a slower loss rate with OH). Reaction with OH is responsible for 26% of the isoprene nitrate loss in BASE, and 21% in simulations with a slower OH reaction rate.

Isoprene nitrates are shown to have a major impact on the NO_x budget in the summertime U.S. boundary layer. Based on constraints from boundary-layer observations, formation of

isoprene nitrates consumes 15-19% of the emitted NO_x (15% in the BASE simulation). Of this amount, deposition of isoprene nitrates permanently removes 8-11% of NO_x emissions (8% in BASE), 3-4% are exported (3% in BASE), and 3-5% are recycled to NO_x (4% in BASE). The large underestimate of ΣAN concentrations in the free troposphere may suggest that export from the boundary layer is underestimated by the model. Through their impact on NO_x, isoprene nitrates also affect ozone concentrations. The observational constraints serve to narrow the uncertainty of this impact on ozone from 4.8 ppbv to 1.8 ppbv.

While we used available observations to constrain uncertainties in isoprene nitrate chemistry, many uncertainties still exist and require further investigation. Our model budgets indicate that the reaction of isoprene with NO_3 is the major pathway for isoprene nitrate formation, but this pathway remains highly uncertain. The NO_3 pathway has not typically been considered important for isoprene because of the diurnal anticorrelation between isoprene (which peaks during mid-day) and NO_3 (which peaks at night). Since this pathway produces organic nitrates with a much higher yield than the OH pathway (in our mechanism, ~80% yield versus 4-8% for the OH pathway), however, it can contribute significantly to isoprene nitrate production even though it is only a minor pathway for isoprene loss (~6% in our model). We also find that our model results are highly sensitive to the degree of recycling of NO_x from the reaction of isoprene nitrates with OH. The amount of NO_x produced from this reaction, and the nature and fate of the multifunctional organic nitrates formed, need further investigation. Finally, the large discrepancy between simulated and observed ΣAN in the free troposphere suggests a shortcoming in the representation of organic nitrates chemistry and/or vertical mixing in the

model mechanism. Based on the available measurements, it is not yet known whether these "missing" nitrates are isoprene nitrates, or nitrates derived from other parent hydrocarbons.

References

Aschmann, S.M., R. Atkinson, and J. Arey (2002), Products of reaction of OH radicals with a-pinene, *J. Geophys. Res.*, *107*(D14), 4191, doi:10.1029/2001JD001098.

Bey, I., D.J. Jacob, R.M. Yantosca, J.A. Logan, B.D. Field, A.M. Fiore, Q. Li, H.Y. Liu, L.J. Mickley, and M.G. Schultz (2001), Global modeling of tropospheric chemistry with assimilated meteorology: Model description and evaluation, *J. Geophys. Res.*, *106*, 23,073-23,095.

Blake, N.J., and 16 others (2003), NMHCs and halocarbons in Asian continental outflow during the Transport and Chemical Evolution over the Pacific (TRACE-P) Field Campaign: Comparison With PEM-West B, *J. Geophys. Res.*, *108*(D20), 8806, doi:10.1029/2002JD003367.

Brune, W.H., X. Ren, J. Mao, R. Lesher, R. Long,. J. Crawford, G. Chen, J. Olson, R. Cohen, B. Heike, H.C. Singh, A. Fred, et al. (2006), HO_x chemistry and ozone production in the different plumes encountered during INTEX-A, to be submitted to *J. Geophys. Res.*.

Chen, X., D. Hulbert, and P.B. Shepson (1998), Measurement of the organic nitrate yield from OH reaction with isoprene, *J. Geophys. Res.*, *103*(D19), 25,563-25,568.

Chuong B., and P. S. Stevens (2002), Measurements of the kinetics of the OH-initiated oxidation of isoprene, *J. Geophys. Res.*, *107*(D13), 4162, doi:10.1029/2001JD000865.

Cleary, P.A., J.G. Murphy, P.J. Wooldridge, D.A. Day, D.B. Millet, M. McKay, A.H. Goldstein, and R.C. Cohen (2005), Observations of total alkyl nitrates within the Sacramento Urban Plume, *Atmos. Chem. Phys. Discuss.*, *5*, 4801-4843.

Crounse, J., P. Wennberg, et al. (2006), Peroxyacetic acid is ubiquitous in the upper troposphere, to be submitted to *J. Geophys. Res.*.

Day, D.A., P.J. Wooldridge, M. Dillon, J.A. Thornton, and R.C. Cohen (2002), A thermal dissociation-laser induced fluorescence instrument for in-situ detection of NO_2, peroxy(acyl)nitrates, alkyl nitrates, and HNO_3., *J. Geophys. Res.*, *107*(D6), 10.1029/2001JD000779.

Day, D.A., M.B. Dillon, P.J. Wooldridge, J.A. Thornton, R.S. Rosen, E.C. Wood, and R.C. Cohen (2003), On Alkyl Nitrates, Ozone and the 'Missing NO_y', *J. Geophys. Res.*, *108*(D16), 10.1029/2003JD003685.

de Gouw, J.A., P.D. Goldan, C. Warneke, W.C. Kuster, J.M. Roberts, M. Marchewka, S.B. Bertman, A.A.P. Pszenny, and W.C. Keene (2003), Validation of proton transfer reaction-mass spectrometry (PTR-MS) measurements of gas-phase organic compounds in

the atmosphere during the New England Air Quality Study (NEAQS) in 2002, *J. Geophys. Res.*, *108*(D21), 4682, doi:10.1029/2003JD003863.

de Gouw, J.A., C. Warneke, A. Stohl, A.G. Wollny, C.A. Brock, O.R. Cooper, J.S. Holloway, M. Trainer, F.C. Fehsenfeld, E.L. Atlas, S.G. Donnelly, V. Stroud, and A. Lueb (2006), The VOC composition of aged forest fire plumes from Alaska and western Canada, *J. Geophys. Res.*, *111*, D10303, doi:10.1029/2005JD006175.

Fan, J., and R. Zhang, Atmospheric oxidation mechanism of isoprene (2004), *Environ. Chem.*, *1*, 140-149, doi:10.1071/EN04045.

Fehsenfeld, F.C., et al. (2006), International Consortium for Atmospheric Research on Transport and Transformation (ICARTT): North America to Europe: Overview of the 2004 summer field study, to be submitted to *J. Geophys. Res.*.

Fiore, A. M., L. W. Horowitz, D. W. Purves, H. Levy II, M. J. Evans, Y. Wang, Q. Li, and R. M. Yantosca (2005), Evaluating the contribution of changes in isoprene emissions to surface ozone trends over the eastern United States, *J. Geophys. Res.*, *110*, D12303, doi:10.1029/2004JD005485.

Fried, A., J. Walega, J. Olson, J. Crawford, G. Chen, B. Heikes, D. O'Sullivan, H. Shen, et al. (2006), The role of convection in redistributing formaldehyde to the upper troposphere

over North America and the North Atlantic during the Summer 2004 INTEX campaign, to be submitted to *J. Geophys. Res.*.

Giacopelli, P., K. Ford, C. Espada, and P.B. Shepson (2005), Comparison of the measured and simulated isoprene nitrate distributions above a forest canopy, *J. Geophys. Res.*, *110*, D01304, doi:10.1029/2004JD005123.

Grossenbacher, J.W., T. Couch, P.B. Shepson, T. Thornberry, M. Witmer-Rich, M.A. Carroll, I. Faloona, D. Tan, W. Brune, K. Ostling, and S. Bertman (2001), Measurements of isoprene nitrates above a forest canopy, *J. Geophys. Res.*, *106*(D20), 24,429-24,438.

Grossenbacher, J.W., D.J. Barket Jr., P.B. Shepson, M.A. Carroll, K. Olszyna, and E. Apel (2004), A comparison of isoprene nitrate concentrations at two forest-impacted sites, *J. Geophys. Res.*, *109*, D11311, doi: 10.1029/2003JD003966.

Guenther, A., C.N. Hewitt, D. Erickson, R. Fall, C. Geron, T. Graedel, P. Harley, L. Klinger, M. Lerdau, W.A. McKay, T. Pierce, B. Scholes, R. Steinbrecher, R. Tallamraju, J. Taylor, and P. Zimmerman (1995), A global model of natural volatile organic carbon emissions, *J. Geophys. Res.*, *100*, 8873-8892.

Guenther, A., T. Karl, P. Harley, C. Wiedinmyer, P. I. Palmer, C. Geron (2006), Estimates of global terrestrial isoprene emissions using MEGAN (Model of Emissions of Gases and Aerosols from Nature), *Atmos. Chem. Phys. Discuss.*, *6*, 107-173.

Holloway, J.S., R.O. Jakoubek, D.D. Parrish, C. Gerbig, A. Volz-Thomas, S. Schmitgen, A. Fried, B. Wert, B. Henry, and J.R. Drummond (2000), Airborne intercomparison of vacuum ultraviolet fluorescence and tunable diode laser absorption measurements of tropospheric carbon monoxide, *J. Geophys. Res.*, *105*, 24,251-24,262.

Horowitz, L.W., J. Liang, G.M. Gardner, and D.J. Jacob (1998), Export of reactive nitrogen from North America during summertime: Sensitivity to hydrocarbon chemistry, *J. Geophys. Res.*, *103*, 13,451– 13,476.

Horowitz, L.W., S. Walters, D.L. Mauzerall, L.K. Emmons, P.J. Rasch, C. Granier, X.X. Tie, J.-F. Lamarque, M.G. Schultz, G.S. Tyndall, J.J. Orlando, and G.P. Brasseur (2003), A global simulation of tropospheric ozone and related tracers: Description and evaluation of MOZART, version 2, *J. Geophys. Res.*, *108*(D24), 4784, doi:10.1029/2002JD002853.

Houweling, S., F. Dentener, and J. Lelieveld (1998), The impact of non-methane hydrocarbon compounds on tropospheric photochemistry, J. Geophys. Res., 103, 10,673-10,696.

Kwok, E.S.C., and R. Atkinson (2005), Estimation of hydroxyl radical reaction rate constants for gas-phase organic compounds using a structure-reactivity relationship: An update, *Atmos. Environ.*, *29*, 1685-1695.

Madronich, S., and S. Flocke (1998), The role of solar radiation in atmospheric chemistry, in *Handbook of Environmental Chemistry*, edited by P. Boule, pp. 1-26, Springer-Verlag, New York.

Neeb, P. (2000), Structure-reactivity based estimation of the rate constants for hydroxyl radical reactions with hydrocarbons, *J. Atmos. Chem.*, *35*, 295-315.

Nozière, B., I. Barnes, and K. Becker (1999), Product study and mechanisms of the reactions of α-pinene and of pinonaldehyde with OH radicals, *J. Geophys. Res.*, *104*(D19), 23,645-23,656.

Paulson, S.E. and J.H. Seinfeld (1992), Development and evaluation of a photooxidation mechanism for isoprene, *J. Geophys. Res.*, *97*, 20,703-20,715.

Pierce, T., C. Geron, L. Bender, R. Dennis, G. Tonnesen, and A. Guenther (1998), Influence of increased isoprene emissions on regional ozone modeling, *J. Geophys. Res.*, *103*, 25,611-25,629.

Pöschl, U., R. von Kuhlmann, N. Poisson, and P.J. Crutzen (2000), Development and intercomparison of condensed isoprene oxidation mechanisms for global atmospheric modeling, *J. Atmos. Chem.*, *37*, 29-52.

Purves, D.W., J.P. Caspersen, P.R. Moorcroft, G.C. Hurtt, and S.W. Pacala (2004), Human-induced changes in U.S. biogenic VOC emissions: Evidence from long-term forest inventory data, *Global Change Biol.*, *10*, 1-19, doi:10.1111/j.1365-2486.2004.00844.x.

Roller, C., A. Fried, J. Walega, P. Weibring, and F. Tittel (2006), Advances in hardware, system diagnostics software, and acquisition procedures for high performance airborne tunable diode laser measurements of formaldehyde, *Appl. Phys. B*, *82*, 247-264, doi:10.1007/s00340-005-1998-8.

Rosen, R.S., E.C. Wood, P.J. Wooldridge, J.A. Thornton, D.A. Day, W. Kuster, E.J. Williams, B.T. Jobson, and R.C. Cohen (2004), Observations of total alkyl nitrates during Texas Air Quality Study 2000: Implications for O_3 and alkyl nitrate photochemistry, *J. Geophys. Res.*, *109*(D7), D07303, doi:10.1029/2003JD004227.

Ryerson, T.B., and 30 others (2003), Effect of petrochemical industrial emissions of reactive alkenes and NO_x on tropospheric ozone formation in Houston, Texas, *J. Geophys. Res.*, *108*(D8), 4249, doi:10.1029/2002JD003070.

Sachse, G. W., G.F. Hill, L.O. Wade, and M.G. Perry (1987), Fast-response, high-precision carbon monoxide sensor using a tunable diode laser absorption technique, *J. Geophys. Res.*, *92*, 2071-2081.

Shepson, P.B., E. Mackay, and K. Muthuramu (1996), Henry's law constants and removal processes for several atmospheric β-hydroxy alkyl nitrates, *Enivron. Sci. Technol.*, *30*, 3618-3623.

Shim, C., Wang, Y., Choi, Y., Palmer, P., Abbot, D., and Chance, K. (2005), Constraining global isoprene emissions with Global Ozone Monitoring Experiment (GOME) formaldehyde column measurements, *J. Geophys. Res.*, *110*(D24), D24301, doi:10.1029/2004JD005629.

Sillman, S., and P. J. Samson (1995), Impact of temperature on oxidant photochemistry in urban, polluted rural and remote environments, *J. Geophys. Res.*, *100*(D6), 11,497-11,508, 10.1029/94JD02146.

Singh, H., Y. Chen, A. Tabazadeh, Y. Fukui, I. Bey, R. Yantosca, D. Jacob, F. Arnold, K. Wohlfrom, E. Atlas, F. Flocke, D. Blake, N. Blake, B. Heikes, J. Snow, R. Talbot, G. Gregory, G. Sachse, S. Vay, and Y. Kondo (2000), Distribution and fate of selected oxygenated organic species in the troposphere and lower stratosphere over the Atlantic, *J. Geophys. Res.*, *105*(D3), 3795-3806.

Singh H.B., W. Brune, J. Crawford, and D. Jacob (2006a), Overview of the Summer 2004 Intercontinental Chemical Transport Experiment-North America (INTEX-A), to be submitted to *J. Geophys. Res.*.

Singh, H.B., L. Salas, D. Herlth, R. Kolyer, E. Czech, M. Avery, J.H. Crawford, G.W. Sachse, D.R. Blake, R.C. Cohen, J. Dibb, G. Huey, R.C. Hudman, D.J. Jacob, L.K. Emmons, L.W. Horowitz, F. Flocke, Y. Tang, and G.R. Carmichael (2006b), Reactive nitrogen distribution and partitioning in the North American troposphere and lowermost stratosphere, submitted to *J. Geophys. Res.*.

Slusher, D. L., L. G. Huey, D. J. Tanner, F. M. Flocke, and J. M. Roberts (2004), A thermal dissociation-chemical ionization mass spectrometry (TD-CIMS) technique for the simultaneous measurement of peroxyacyl nitrates and dinitrogen pentoxide, *J. Geophys. Res., 109*, D19315, doi:10.1029/2004JD004670.

Sprengnether, M., K.L. Demerjian, N.M. Donahue, and J.G. Anderson (2002), Product analysis of the OH oxidation of isoprene and 1,3-butadiene in the presence of NO, *J. Geophys. Res., 107*(D15), doi:10.1029/2001JD000716.

Thornton, J.A., P.J. Wooldridge, and R.C. Cohen Atmospheric NO_2: In situ laser-induced fluorescence detection at parts per trillion mixing ratios (2000), *Anal. Chem., 72*, 528-539, doi:10.1021/ac9908905.

Trainer, M., E.J. Williams, D.D. Parrish, M.P. Buhr, E.J. Allwine, H.H. Westberg, F.C. Fehsenfeld, and S.C. Liu (1987), Models and observations of the impact of natural hydrocarbons on rural ozone, *Nature, 329*, 705-707.

Trainer, M., M.P. Buhr, C.M. Curran, F.C. Fehsenfeld, E.Y. Hsie, S.C. Liu, R.B. Norton, D.D. Parrish, E.J. Williams, B.W. Gandrud, B.A. Ridley, J.D. Shetter, E.J. Allwine, and H.H. Westberg, Observations and modeling of the reactive nitrogen photochemistry at a rural site, *J. Geophys. Res.*, *96*(D2), 3045-3063, 1991.

Treves, K., and Y. Rudich, The atmospheric fate of C_3-C_6 hydroxyalkyl nitrates (2003), *J. Phys. Chem. A*, *107*, 7809-7817.

Turquety, S., J.A. Logan, D.J. Jacob, R.C. Hudman, F.Y. Leung, C.L. Heald, R.M. Yantosca, S. Wu, L.K. Emmons, D.P. Edwards, and G.W. Sachse (2006), Inventory of boreal fire emissions for North America in 2004: The importance of peat burning and pyro-convective injection, submitted to *J. Geophys. Res.*.

Vay, S.A., B.E. Anderson, G.W. Sachse, J.E. Collins Jr., J.R. Podolske, C.H. Twohy, B. Gandrud, K.R. Chan, S.L. Baughcum, and H.A. Wallio (1998), DC-8-based observations of aircraft CO, CH_4, N_2O, and H_2O(g) emission indices during SUCCESS, *Geophys. Res. Lett.*, *25*, 1717-1720.

von Kuhlmann, R., M.G. Lawrence, U. Pöschl, and P.J. Crutzen (2004), Sensitivities in global scale modeling of isoprene, *Atmos. Chem. Phys.*, *4*, 1-17.

Wu, S., L.J. Mickley, D.J. Jacob, J.A. Logan, R.M. Yantosca, and D. Rind (2006), Why are there large differences between models in global budgets of tropospheric ozone?, submitted to *J. Geophys. Res.*.

Table 1. Isoprene and monoterpene mechanism used in base model simulations. Second-order reaction rate constants are given in units of molec^{-1} cm^3 s^{-1}.

Reaction	**Rate Constant**
ISOP + OH → ISOPO2	2.54E-11*exp(410/T)
ISOP + O3 → .4*MACR + .2*MVK + .07*C3H6 + .27*OH + .06*HO2 + .6*CH2O + .3*CO + .1*O3 + .2*MCO3 + .2*CH3COOH	1.05E-14*exp(-2000/T)
ISOP + NO3 → ISOPNO3	3.03E-12*exp(-446/T)
ISOPO2 + NO → .04*ONITR + .96*NO2 + HO2 + .57*CH2O + .24*MACR + .33*MVK + .38*HYDRALD	2.20E-12*exp(180/T)
ISOPO2 + NO3 → HO2 + NO2 + .6*CH2O + .25*MACR + .35*MVK + .4*HYDRALD	2.40E-12
ISOPO2 + HO2 → ISOPOOH	8.00E-13*exp(700/T)
ISOPO2 + CH3O2 → .25*CH3OH + HO2 + 1.2*CH2O + .19*MACR + .26*MVK + .3*HYDRALD	5.00E-13*exp(400/T)
ISOPO2 + CH3CO3 → CH3O2 + HO2 + .6*CH2O + .25*MACR + .35*MVK + .4*HYDRALD	1.40E-11
MVK + hv → .7*C3H6 + .7*CO + .3*CH3O2 + .3*CH3CO3	Photolysis
MVK + OH → MACRO2	4.13E-12*exp(452/T)
MVK + O3 → .8*CH2O + .95*CH3COCHO + .08*OH + .2*O3 + .06*HO2 + .05*CO + .04*CH3CHO	7.52E-16*exp(-1521/T)
MACR + hv → .67*HO2 + .33*MCO3 + .67*CH2O + .67*CH3CO3 + .33*OH + .67*CO	Photolysis
MACR + OH → .5*MACRO2 + .5*H2O + .5*MCO3	1.86E-11*exp(175/T)
MACR + O3 → .8*CH3COCHO + .275*HO2 + .2*CO + .2*O3 + .7*CH2O + .215*OH	4.40E-15*exp(-2500/T)

Reaction	Rate Constant
MACRO2 + NO → NO2 + .47*HO2 + .25*CH2O + .25*CH3COCHO + .53*CH3CO3 + .53*GLYALD + .22*HYAC + .22*CO	2.70E-12*exp(360/T)
MACRO2 + NO → ONITR	1.30E-13*exp(360/T)
MACRO2 + NO3 → NO2 + .47*HO2 + .25*CH2O + .25*CH3COCHO + .22*CO + .53*GLYALD + .22*HYAC + .53*CH3CO3	2.40E-12
MACRO2 + HO2 → MACROOH	8.00E-13*exp(700/T)
MACRO2 + CH3O2 → .73*HO2 + .88*CH2O + .11*CO + .24*CH3COCHO + .26*GLYALD + .26*CH3CO3 + .25*CH3OH + .23*HYAC	5.00E-13*exp(400/T)
MACRO2 + CH3CO3 → .25*CH3COCHO + CH3O2 + .22*CO + .47*HO2 + .53*GLYALD + .22*HYAC + .25*CH2O + .53*CH3CO3	1.40E-11
ISOPOOH + hv → .402*MVK + .288*MACR + .69*CH2O + HO2	Photolysis
ISOPOOH + OH → .5*XO2 + .5*ISOPO2	3.80E-12*exp(200/T)
MACROOH + OH → .5*MCO3 + .2*MACRO2 + .1*OH + .2*HO2	2.30E-11*exp(200/T)
ONITR + hv → HO2 + CO + NO2 + CH2O	Photolysis
ONITR + OH → .4*HYDRALD + .4*NO2 + HO2 + .6*XNITR	4.50E-11
ONITR + NO3 → NO2 + HO2 + XNITR	1.40E-12*exp(-1860/T)
ISOPNO3 + NO → 1.206*NO2 + .794*HO2 + .072*CH2O + .167*MACR + .039*MVK + .794*ONITR	2.70E-12*exp(360/T)
ISOPNO3 + NO3 → 1.206*NO2 + .072*CH2O + .167*MACR + .039*MVK + .794*ONITR + .794*HO2	2.40E-12
ISOPNO3 + HO2 → .206*NO2 + .794*HO2 + .008*CH2O + .167*MACR + .039*MVK + .794*ONITR	8.00E-13*exp(700/T)

Reaction	**Rate Constant**
C10H16 + OH → TERPO2	1.20E-11*exp(444/T)
C10H16 + O3 → .7*OH + MVK + MACR + HO2	1.00E-15*exp(-732/T)
C10H16 + NO3 → TERPO2 + NO2	1.20E-12*exp(490/T)
TERPO2 + NO → .1*CH3COCH3 + HO2 + .82*MVK + .82*MACR + .82*NO2 + .18*ONITR	4.20E-12*exp(180/T)
TERPO2 + HO2 → TERPOOH	7.50E-13*exp(700/T)
TERPOOH + hv → OH + .1*CH3COCH3 + HO2 + MVK + MACR	Photolysis
TERPOOH + OH → TERPO2	3.80E-12*exp(200/T)

Table 2. Sensitivity simulations in MOZART-4 model.

Simulation	**Yield[1]**	**Loss rate[2]**	**Deposition[3]**	**NO_x recycling[4]**	**Isoprene nitrate burden[5] (GgN)**	**Isoprene nitrate lifetime[6] (hrs)**
4% (BASE)	4%	Fast	Fast	40%	1.57	15.0
4%_slowOH	4%	Slow	Fast	40%	1.69	16.2
4%_slowDD	4%	Fast	Slow	40%	3.20	30.3
8%	8%	Fast	Fast	40%	1.94	15.1
8%_slowOH	8%	Slow	Fast	40%	2.10	16.5
8%_slowDD	8%	Fast	Slow	40%	3.95	30.5
4%_0%NOx	4%	Fast	Fast	0%	2.26	21.8
4%_100%NOx	4%	Fast	Fast	100%	0.49	4.6
8%_slowOH_100%NOx	8%	Slow	Fast	100%	0.89	6.8

[1]Yield of isoprene nitrates (ONITR) from the reaction of isoprene peroxy radicals (ISOPO2) with NO.

[2]Loss rates of ONITR. "Fast" indicates $k(OH+ONITR) = 4.5x10^{-11}$ $molec^{-1}$ cm^3 s^{-1}, $J(ONITR) = J(CH_3CHO)$. "Slow" indicates $k(OH+ONITR) = 1.3x10^{-11}$, $J(ONITR) = J(HNO_3)$.

[3]Rate of ONITR dry deposition. "Fast" indicates $V_d(ONITR) = V_d(HNO_3)$. "Slow" indicates $V_d(ONITR) = V_d(PAN)$. In both cases, wet deposition is based on a Henry's Law constant of $H_{298}(ONITR) = 7.51x10^3$ M atm^{-1}.

[4]Recycling of NO_x from reaction of ONITR+OH. The balance of the reactive nitrogen produces multifunctional organic nitrates (XNITR).

[5]Mean burden of isoprene nitrates (ONITR+XNITR+ISOPNO3) in the eastern United States (24-52°N, 62.5-97.5°W) boundary layer (below 800 hPa) during July 2004.

[6]Mean lifetime of isoprene nitrates (ONITR+XNITR+ISOPNO3) in the eastern United States boundary layer during July 2004 versus all loss processes shown in Figure 2.

Figure Captions

Figure 1. MOZART-4 model versus observed concentrations of selected trace species for daytime observations (1500-2300 UTC) below 2 km. Hourly model results are sampled at the locations of 1-minute observations. The 1-minute model values and observations for each NOAA WP-3D and NASA DC-8 flight are then averaged onto the model grid. Observations shown from the NASA DC-8 are: ozone (PI: Avery, chemiluminescence), CO (PI: Sachse differential absorption TDL spectrometer) [*Sachse et al.*, 1987; *Vay et al.*, 1998]), isoprene (PI: D. Blake, whole-air sample, gas chromatography) [*Blake et al.*, 2003], NO_x = NO (PI: Brune) [*Brune et al.*, 2006] + NO_2 (PI: Cohen, laser induced fluorescence) [*Thornton et al.*, 2000], PAN (PI: Singh, electron-capture gas chromatography) [*Singh et al.*, 2000, 2006b], HNO_3 and H_2O_2 (PI: Wennberg, chemical ionization mass spectrometer) [*Crounse et al.*, 2006], total alkyl- and hydroxyalkyl-nitrates (AN, PI: Cohen, thermal dissociation - laser induced fluorescence) [*Day et al.*, 2002; *Cleary et al.*, 2005] and CH_2O (PI: Fried, TDLAS) [*Roller et al.*, 2006, and references therein; *Fried et al.*, 2006]. Observations shown from the NOAA WP-3D are: ozone (PI: Ryerson, chemiluminescence) [*Ryerson et al.*, 2003], CO (PI: Holloway, vacuum UV fluorescence) [*Holloway et al.*, 2000], isoprene, methylvinyl ketone + methacrolein (MVK+MACR), and monoterpenes (PIs: de Gouw and Warneke, PTR-MS) [*de Gouw et al.*, 2003, 2006], and PAN (PI: Flocke, thermal dissociation-chemical ionization mass spectrometry) [*Slusher et al.*, 2004].

Figure 2. Budgets of isoprene nitrates (ONITR+XNITR+ISOPNO3) in the eastern United States (24-52°N, 62.5-97.5°W) boundary layer (below 800 hPa) during July 2004 for each model simulation. Production of isoprene nitrates occurs from terpenes (pinene), methylvinyl ketone and methacrolein (MACR), and from isoprene reactions with NO3 (NO3) and OH (ISOP). Loss occurs via photolysis and vertical diffusion (hv+DIF), reaction with OH (OH), wet deposition (WD), advection (ADV), convection (CNV), and dry deposition (DD).

Figure 3. Mean ICARTT vertical profile of the sum of all alkyl nitrates (ΣAN) from observations (black, standard deviations indicated by horizontal bars) and model (colored by simulation as shown in legend; see also Table 2) from all DC-8 flights (left). Correlation plot of ozone versus ΣAN and reduced major axis regression line from observations (black points and line) and model (colored points and lines) for daytime (1500-2300 UTC) DC-8 data over the eastern United States (24-52°N, 62.5-97.5°W) (right). Hourly model results are sampled at the locations of the 1-minute observations. In the ozone-ΣAN correlation plot, 1-minute data points for each flight have been averaged onto the model grid.

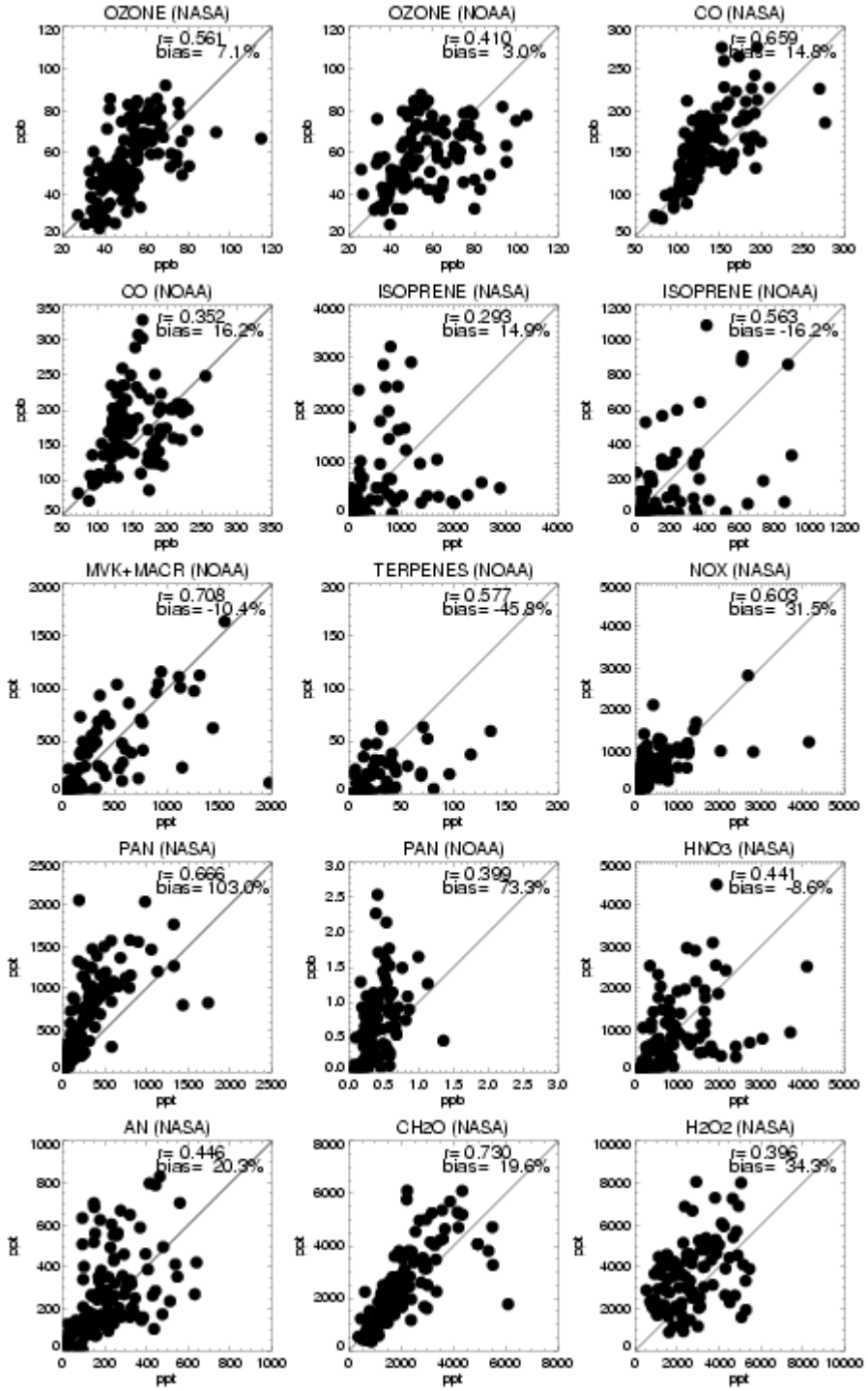

Figure 1. MOZART-4 model versus observed concentrations of selected trace species for daytime observations (1500-2300 UTC) below 2 km. Hourly model results are sampled at the locations of 1-minute observations. The 1-minute model values and observations for each NOAA

WP-3D and NASA DC-8 flight are then averaged onto the model grid. Observations shown from the NASA DC-8 are: ozone (PI: Avery, chemiluminescence), CO (PI: Sachse differential absorption TDL spectrometer) [*Sachse et al.*, 1987; *Vay et al.*, 1998]), isoprene (PI: D. Blake, whole-air sample, gas chromatography) [*Blake et al.*, 2003], NO_x = NO (PI: Brune) [*Brune et al.*, 2006] + NO_2 (PI: Cohen, laser induced fluorescence) [*Thornton et al.*, 2000], PAN (PI: Singh, electron-capture gas chromatography) [*Singh et al.*, 2000, 2006b], HNO_3 and H_2O_2 (PI: Wennberg, chemical ionization mass spectrometer) [*Crounse et al.*, 2006], total alkyl- and hydroxyalkyl-nitrates (AN, PI: Cohen, thermal dissociation - laser induced fluorescence) [*Day et al.*, 2002; *Cleary et al.*, 2005] and CH_2O (PI: Fried, TDLAS) [*Roller et al.*, 2006, and references therein; *Fried et al.*, 2006]. Observations shown from the NOAA WP-3D are: ozone (PI: Ryerson, chemiluminescence) [*Ryerson et al.*, 2003], CO (PI: Holloway, vacuum UV fluorescence) [*Holloway et al.*, 2000], isoprene, methylvinyl ketone + methacrolein (MVK+MACR), and monoterpenes (PIs: de Gouw and Warneke, PTR-MS) [*de Gouw et al.*, 2003, 2006], and PAN (PI: Flocke, thermal dissociation-chemical ionization mass spectrometry) [*Slusher et al.*, 2004].

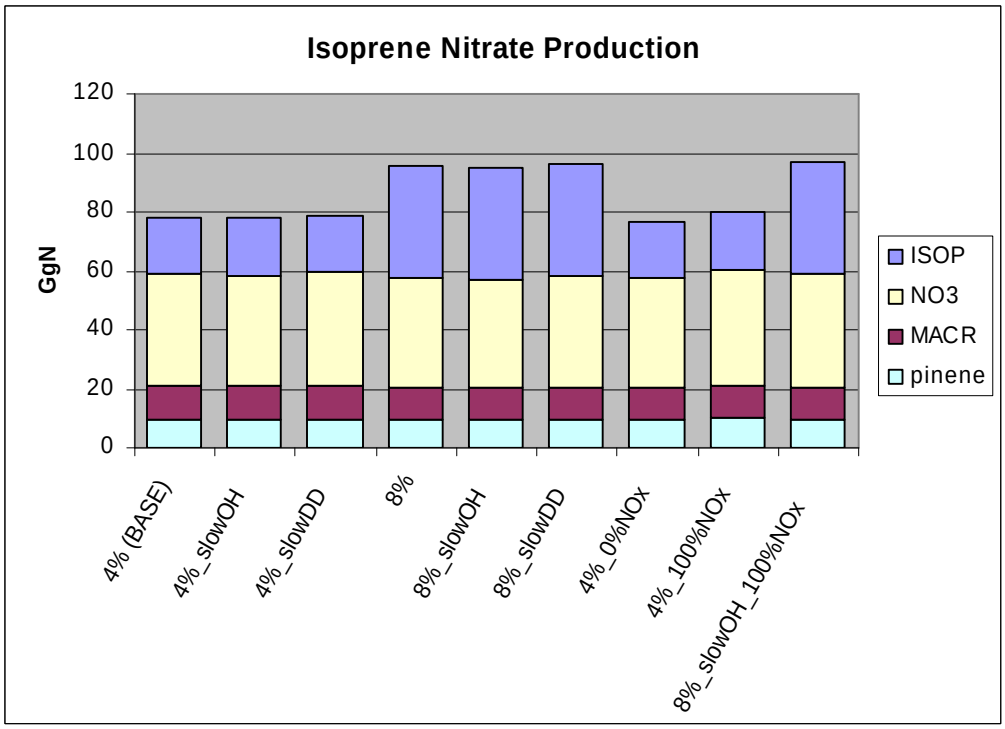

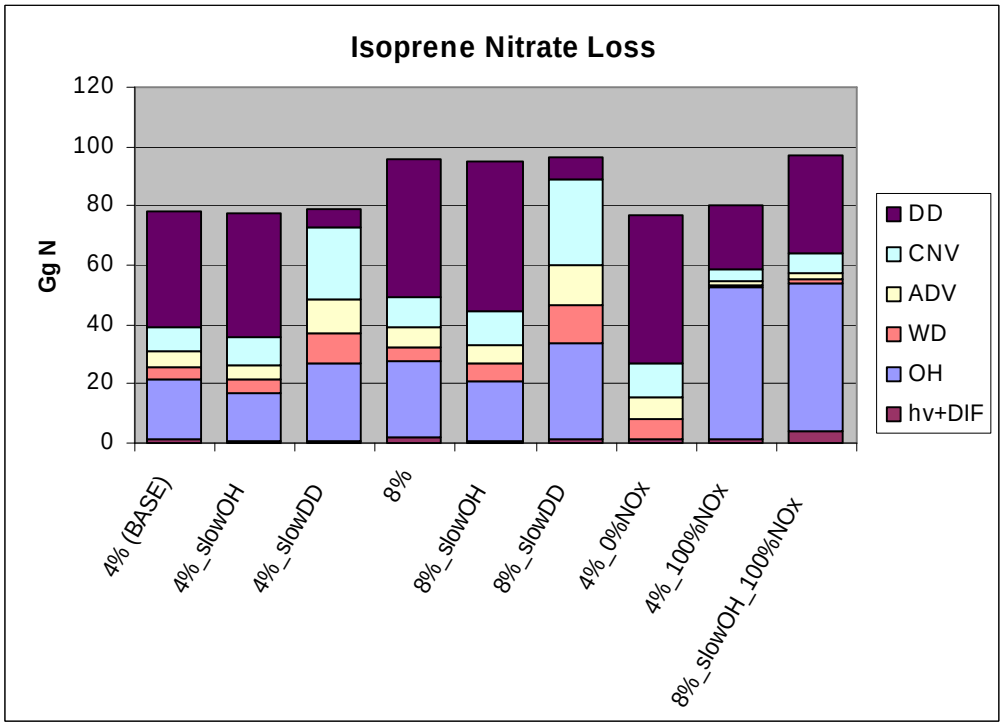

Figure 2. Budgets of isoprene nitrates (ONITR+XNITR+ISOPNO3) in the eastern United States (24-52°N, 62.5-97.5°W) boundary layer (below 800 hPa) during July 2004 for each model

simulation (Table 2). Production of isoprene nitrates occurs from terpenes (pinene), methylvinyl ketone and methacrolein (MACR), and from isoprene reactions with NO_3 (NO3) and OH (ISOP). Loss occurs via photolysis and vertical diffusion (hv+DIF), reaction with OH (OH), wet deposition (WD), advection (ADV), convection (CNV), and dry deposition (DD).

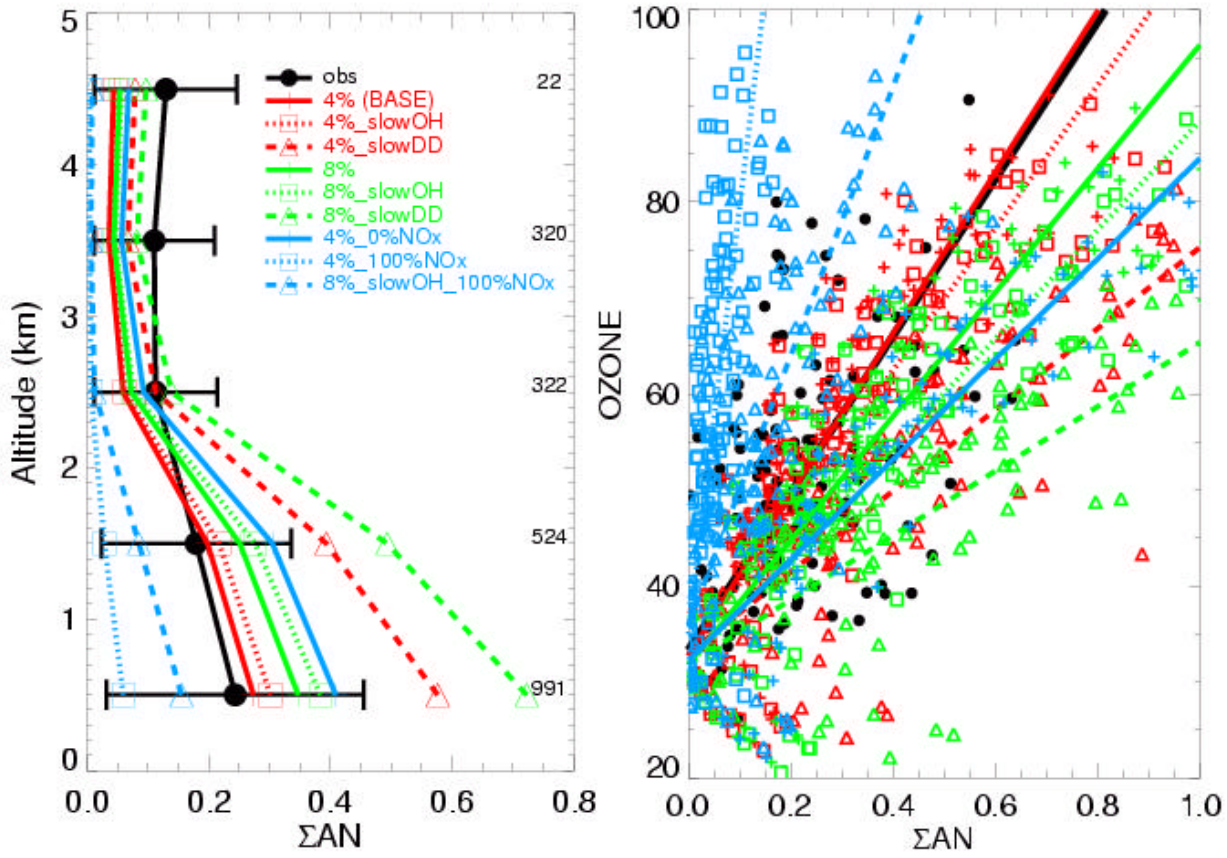

Figure 3. Mean ICARTT vertical profile of the sum of all alkyl nitrates (ΣAN) from observations (black, standard deviations indicated by horizontal bars) and model (colored by simulation as shown in legend; see also Table 2) from all DC-8 flights (left). Correlation plot of ozone versus ΣAN and reduced major axis regression line from observations (black points and line) and model (colored points and lines) for daytime (1500-2300 UTC) DC-8 data over the eastern United States (24-52°N, 62.5-97.5°W) (right). Hourly model results are sampled at the locations of the 1-minute observations. In the ozone-ΣAN correlation plot, 1-minute data points for each flight have been averaged onto the model grid.